An adaptive supramolecular hydrogel comprising a self-sorting double nanofibre network

Hajime Shigemitsu[1,†], Takahiro Fujisaku[1], Wataru Tanaka[1], Ryou Kubota[1], Saori Minami[2], Kenji Urayama[2], Itaru Hamachi[1,3]*

[1]Department of Synthetic Chemistry and Biological Chemistry, Graduate School of Engineering, Kyoto University, Katsura, Kyoto 615-8510, JAPAN

[2]Department of Macromolecular Science and Engineering, Kyoto Institute of Technology, Matsugasaki, Kyoto 606-8585, JAPAN

[3]Core Research for Evolutional Science and Technology (CREST), Japan Science and Technology Agency (JST), 5 Sanbancho, Chiyoda-ku, Tokyo 102-0075, JAPAN

[†]Present address: Department of Applied Chemistry, Graduate School of Engineering, Osaka University, 2-1 Yamadaoka, Suita, Osaka 565-0871, JAPAN

Correspondence: ihamachi@sbchem.kyoto-u.ac.jp

Abstract

Novel soft materials should comprise multiple supramolecular nanostructures whose responses (*e.g.* assembly and disassembly) to external stimuli can be controlled independently. Such multicomponent systems are present in living cells and control the formation and breaking up of a variety of supramolecular assemblies made of proteins, lipids, DNA and RNA in response to external stimuli; however, artificial counterparts are challenging to make. Here, we present a hybrid hydrogel consisting of a self-sorting double network (SDN) of nanofibres in which each network responds to an applied external stimulus independent of the other. The hydrogel can be made to change its mechanical properties and rates of release of encapsulated proteins by adding $Na_2S_2O_4$ or bacterial alkaline phosphatase (BAP). Notably, the properties of the gel depend on the order in which the external stimuli are applied. Multicomponent hydrogels comprising orthogonal stimulus-responsive supramolecular assemblies would be suitable for designing novel adaptive materials.

Main text

In living systems, a myriad of biomolecules such as proteins, lipids, DNA, and RNA spontaneously form distinct supramolecular assemblies through noncovalent interactions.[1] These assemblies are diverse and orthogonal and their formation and collapse are precisely regulated, which is crucial for the multifunctionality and autonomy of living cells. Fibrous supramolecular assemblies of cells (*e.g.*, actin filaments, and microtubules) respond to various chemical and physical stimuli (*e.g.*, pH, mechanical stress, and biomolecules), and dynamic structural changes are closely involved in the mechanical support of live cells, their metamorphosis, and migration.[2] Given such sophisticated natural systems, the controlled hybridisation of multiple supramolecular assemblies bearing orthogonal functionality is expected to produce novel artificial soft materials.[3–19] Self-sorting events and orthogonal assemblies of synthetic molecules are among the key factors for the construction of ordered systems made of multiple supramolecular structures. van Esch and co-workers pioneered the demonstration of hybrid supramolecular hydrogels by orthogonally encapsulating vesicles that contained enzymes.[20] Adams and co-workers prepared a self-sorting double network (SDN) by applying gradually changing the pH.[21] They subsequently developed SDN hydrogels that can be spatially resolved using UV light.[22] Smith and co-workers also reported a phototuneable SDN hydrogel containing a photo acid generator.[23] Additionally, catalytically incompatible groups can be incorporated into self-sorting nanofibres to achieve multi-step reactions that would not be possible in solution.[24] Self-sorting n-type and p-type supramolecular nanofibres can be assembled for new electrical properties.[25,26] The preparation of supramolecular assemblies/polymer hybrid materials has also been reported.[27] However, the development of hybrid systems composed of supramolecules responsive to

multiple (and orthogonal) stimuli still remains challenging. Such adaptive supramolecular materials exhibiting multiple and unique responses to chemical/biological stimuli could open up the next generation of smart materials for a variety of applications. Their design strategy has not yet well been explored, unlike materials that rely on co-assembly.

Herein, we discovered a new self-sorting gelator pair and a supramolecular hydrogel comprising a stimulus-responsive double network (Figure 1a). Two supramolecular nanofibres that form the SDN hydrogel orthogonally responded orthogonally to different stimuli ($Na_2S_2O_4$ and bacterial alkaline phosphatase (BAP)) and the SDN hydrogel showed bidirectional change in the macroscopic rheological properties. Due to the self-sorting of the two nanofibres, each property could be imparted without interference upon mixing. Unprecedented bidirectional rheological changes led to a unique application in the bidirectionally tuneable release of proteins encapsulated in the SDN hydrogel. Furthermore, the SDN hydrogels exhibited the unique adaptive feature of stimulus-order recognition, which was expressed by the macroscopic gel–sol transition.

Exploration and evaluation of self-sorting double nanofibre networks

We recently reported that two distinct supramolecular fibres — **BPmoc-F$_3$**[28] and **Phos-cycC$_6$**[29] — are self-sorting (Figure 1b, Supplementary Figure 1), which could be clearly visualised *in situ* using confocal laser scanning microscopy (CLSM).[30] Our previous study suggested that orthogonal interaction modes between two components may be one of the strategies for self-sorting; various factors such as formation (kinetic) processes are significant in this event.[14,21] In our cases, the large difference in the interaction modes between peptide-type **BPmoc-F$_3$** (mainly governed by π - π interactions and hydrogen bonding) and lipid-type **Phos-cycC$_6$** (through van der Waals interactions and hydrogen bonding) showed preference for self-sorting rather than co-assembly.[31] On the basis of this assumption, we sought to explore a new self-sorting supramolecular fibre pair based on the combination of peptide-type and lipid-type hydrogelators, and found that **NPmoc-FF** derivatives[32,33] — in which the N-terminal group is replaced with a nitrobenzyl from the boronobenzyl of **BPmoc-F$_3$** — can be self-sorted with **Phos-cycC$_6$** (Figure 1b). Orthogonality in the two-component hydrogel comprising **NPmoc-FF** or **NPmoc-F(4-F)F** and **Phos-cycC$_6$** was initially confirmed by circular dichroism (CD) spectroscopy. **NPmoc-F(4-F)F** and **Phos-cycC$_6$** in a single-component system display a different pattern in the assembly-enhanced CD spectra in an aqueous buffer (100 mM HEPES (4-(2-hydroxyethyl)-1-piperazineethanesulfonic acid), pH 8.0) (Figure 2a, b). **NPmoc-F(4-F)F**, in particular, showed characteristic negative Cotton peaks (273 nm), which were derived from the self-assembled β-sheet-like structure (Figure 2a, Supplementary Figure 2). An assembly-enhanced broad peak was also detected at approximately 265 nm (negative Cotton effect) in a viscous solution of **Phos-cycC$_6$** (Figure 2b, Supplementary

Figure 2), which suggested that assemblies were formed even below the critical gelation concentration (CGC). The CD spectrum of a mixture of two components generating self-sorting supramolecular nanofibres should be a simple sum of each component (theoretical CD spectrum). As expected, the experimental CD agreed with the theoretical CD spectrum (Figure 2c). The self-sorting structures were retained throughout the use of varied mixture ratios or concentrations (Supplementary Figure 3). Similarly, the experimental CD spectrum of the **NPmoc-FF** and **Phos-cycC$_6$** mixture corresponded to the sum of the two corresponding CD spectra (Supplementary Figure 4).

Self-sorting of nanofibres in the hydrogels was further confirmed by *in situ* imaging using CLSM.[30,34] To selectively stain **NPmoc-FF** or **NPmoc-F(4-F)F** fibres, we designed and synthesised a fluorescent probe (**NP-Alexa647**) bearing the **NPmoc-FF** moiety as the hydrophobic core and anionic Alexa647 dye in the hydrophilic part (Figure 1b). To image **Phos-cycC$_6$** fibres, **NBD-cycC$_6$** comtaining a core similar to **Phos-cycC$_6$** was employed (Figure 1b). We then checked the staining selectivities of the two probes for the corresponding fibres. As shown in Figure 2d and e, **NP-Alexa647** stained **NPmoc-F(4-F)F** fibres but not **Phos-cycC$_6$** fibres, whereas **NBD-cycC$_6$** stained **Phos-cycC$_6$** fibres but not **NPmoc-F(4-F)F** fibres. With these selective probes, we subsequently sought to visualise the two self-sorting fibres containing **NPmoc-F(4-F)F** and **Phos-cycC$_6$** in the mixed hydrogel (Supplementary Figure 8). The four components, — **NPmoc-F(4-F)F**, **NP-Alexa647**, **Phos-cycC$_6$**, and **NBD-cycC$_6$** — were mixed and the suspension was heated to form a homogeneous solution, followed by cooling to room temperature to form the gel. The resultant hydrogel was observed using CLSM. Images through the channels for Alexa647 and

NBD showed fibrous structures, but their spatial distributions were visibly different. We quantitatively evaluated the self-sorting degree via Pearson's correlation coefficient (r) which is used to measure the strength of a linear association between two variables.[35] The Pearson's correlation coefficients of the merged images were in the range 0.20–0.30, indicating negligible correlation between the two original images (Supplementary Figure 8). In addition, the super-resolution CLSM images with an Airyscan unit (Figure 2f, Supplementary Figure 9) clearly showed distinct fibres in the SDN hydrogel (Pearson's correlation coefficients: –0.25–0.30). The data showed that almost all **NPmoc-F(4-F)F** and **Phos-cycC$_6$** were self-sorted and orthogonally assembled into two distinct supramolecular nanofibres, thereby forming an SDN hydrogel. Fibers of **NPmoc-FF** were too thin to be observed clearly, as shown in Supplementary Figure 10, moreover, the CLSM image of the mixture (**NPmoc-FF**/**Phos-cycC$_6$**/**NP-Alexa647**/**NBD-cycC$_6$**) also did not clearly show self-sorting structures (Supplementary Figure 10). Therefore, we could not clearly observe the self-sorting of **NPmoc-FF** and **Phos-cycC$_6$**, and decided to use **NPmoc-F(4-F)F**.

Stimulus-response behaviours of a single-component NPmoc-F(4-F)F and Phos-cycC_6 networks

Prior to exploring the functions of the hydrogel containing the two-component self-sorting supramolecular nanofibres, we evaluated the response properties of each single component, *i.e.* the **NPmoc-F(4-F)F** hydrogel and **Phos-cycC_6** viscous liquid. As reported previously,[32] the NPmoc moiety was reductively eliminated, causing the gel–sol transition of the **NPmoc-F(4-F)F** hydrogel in response to appropriate reducing reagents such as $Na_2S_2O_4$ (Figure 3a). As shown in Figure 3b, the **NPmoc-F(4-F)F** hydrogel rapidly changed to sol upon addition of $Na_2S_2O_4$. The HPLC analysis showed that >99% **NPmoc-F(4-F)F** was decomposed by $Na_2S_2O_4$ within 10 min (Figure 3c, Supplementary Figure 11); the CD spectrum of the resultant sol did not show a Cotton peak at approximately 273 nm, which was originally detected as a result of the β-sheet-like structure of the **NPmoc-F(4-F)F** nanofibres (Figure 3d). It was clear that **NPmoc-F(4-F)F** nanofibres were destroyed by the chemical reaction with $Na_2S_2O_4$, similar to the case of the **NPmoc-FF** fibres.

We also explored the stimulus-responsiveness of a single-component **Phos-cycC_6** fibres by treating them with bacterial alkaline phosphatase (BAP), an enzyme that hydrolyses organophosphates (Figure 3e). BAP had a clear effect on **Phos-cycC_6** fibres, as demonstrated by the gradual change of the viscous solution of **Phos-cycC_6** (0.15 wt%: below the CGC (0.30 wt%)) to a transparent gel 2 h after the addition of BAP (Figure 3f). The macroscopic sol–gel change observed by the naked eye was consistent with the rheological measurements (Figure 3g, Supplementary Figure 14). The G' value of the **Phos-cycC_6** viscous liquid was already larger than the G'' value before BAP addition, indicating the existence of loosely linked fibres suggested by the CD spectra (Figure 2b). The addition of BAP continuously

increased the G' value for 3 h, whereas the G'' value remained almost constant, resulting in a greater G' (244 Pa) relative to G'' (16 Pa) (tan δ: 0.07). Gelation was attributed to the BAP-catalysed hydrolysis of **Phos-cycC$_6$** to produce hydrophobic **HO-cycC$_6$** (Figure 3e) which is insoluble in the aqueous buffer solution. HPLC product analysis indicated partial conversion of **Phos-cycC$_6$** to **HO-cycC$_6$** (Figure 3h, Supplementary Figure 12), whereby the **Phos-cycC$_6$** fraction gradually decreased with the concurrent increase of **HO-cycC$_6$**. Interestingly, gelation took place when approximately 50% of **Phos-cycC$_6$** was hydrolysed (Supplementary Figure 13).

To examine the detailed mechanism of the BAP-induced gelation of **Phos-cycC$_6$**, we carefully observed changes to the **Phos-cycC$_6$** fibre network using CLSM *in situ* (Supplementary Figure 15). Many fibres were observed even in the viscous liquid state (before BAP addition), which was in agreement with the data from the rheological experiments and CD spectroscopy. The morphology and density of these fibres did not changed substantially after the addition of BAP. However, we found that the fibre fluidity, which was monitored by fluorescent recovery after photobleaching (FRAP) technique,[36,37,38] was greatly altered by the BAP treatment (Supplementary Figure 16). Before the addition of BAP, the bleached fluorescence recovered sufficiently (recovery ratio: 92.1 $\pm$ 4.7%) within 3 min, indicating that the **Phos-cycC$_6$** fibres were fluidic (diffusion coefficient (D): 1.9 $\pm$ 0.4 $\times$ 10^{-3} μm^2/sec). In contrast, the fibres treated with BAP showed negligible fluorescence recovery (recovery ratio: 3.3$\pm$3.3 %), suggesting the presence of less fluidic solid-like fibres. This remarkable difference may be ascribed to surface modification and/or rearrangement of intermolecular hydrogen bonding of the supramolecular fibres by BAP. Additional CD experiments also showed the impact of BAP treatment on the fibres. The

assembly-enhanced CD spectrum was observed before the BAP addition and it remained almost intact with a slight shift of the Cotton peak from 265 to 272 nm (Figure 3i). This strongly suggested that the molecular packing/orientation of the original **Phos-cycC$_6$** fibre was modulated by the BAP-catalysed partial hydrolysis. Detailed experiments (Supplementary Figures 17–20) suggested that 'enzymatic modification of supramolecular assemblies' may be plausible in this case, where the partial conversion of **Phos-cycC$_6$** to **HO-cycC$_6$** by BAP occurred at the supramolecular fibres surfaces and/or ends.

To investigate changes in the gel network more precisely, we used nanobeads with various diameters (70–800 nm) embedded in the network. The movement of nanobeads was traced using CLSM, which allowed us to evaluate the size of meshes formed by entangled supramolecular fibres.[39,40] When the mesh size of the fibrous network was smaller than that of fluorescent beads, Brownian motion of the beads was restricted and stopped, whereas the beads moved freely when the mesh size was larger than that of the beads. When we mixed the beads with the viscous liquid of **Phos-cycC$_6$**, the fluorescent beads and supramolecular fibres could be distinctly visualised, as shown in Figure 4a. Supplementary movie 1 shows representative examples using 300 nm beads, in which the free Brownian motion of the beads in the **Phos-cycC$_6$** sol almost stopped 3 h after the addition of BAP. Figure 4b shows two snapshot images of the 300 nm beads in the **Phos-cycC$_6$** matrix with a 5 min interval of CLSM observations. The positions of almost all the beads changed after 5 min without BAP treatment, whereas the positions of the beads did not change 5 min after the BAP treatment (Figure 4b). These CLSM images indicated that beads 70 nm to 500 nm in diameter moved freely in the viscous liquid of the **Phos-cycC$_6$** fibre network (0.15 wt%) whereas the 800 nm beads did not move. Therefore, the mesh size of the **Phos-cycC$_6$** viscous liquid was between

500 and 800 nm (Figure 4c). In contrast, only 70 nm beads moved freely and beads larger than 200 nm in diameter almost stopped moving after BAP treatment. Figure 4c shows that the bead size critical for turning the Brownian motion on and off shifted from 500–800 to 200–300 nm after the addition of BAP, which implied that the mesh size became smaller. These results consistently demonstrated that a dense cross-linked fibre network was obtained by BAP treatment, which facilitated gelation of the viscous liquid of **Phos-cycC$_6$**.

Bidirectional tuning of rheological properties and protein release profiles of the SDN hydrogel

If the two gelators are co-assembled upon mixing, the original properties of these fibres may interfere, possibly resulting in hybrid fibres showing properties different from the sum of the original ones. In contrast, it is reasonable to expect the programmable construction of a hybrid hydrogel that retains distinct stimulus-responsiveness upon mixing of two fibres if these are orthogonally self-sorted (a possible scenario shown in Figure 5a).

According to this scenario, we prepared a mixed-hydrogel comprising **NPmoc-F(4-F)F** and **Phos-cycC_6** and monitored the stimulus responses. The two-component SDN hydrogel changed to a viscous liquid within 10 min after the addition of $Na_2S_2O_4$ whereas the addition of BAP toughened the hydrogel (Figure 5b). As shown in Figure 5c, the rheological data quantitatively supported the behaviours observed by the naked eye. The G' and G'' values of the SDN hydrogel were respectively 187 and 60 Pa, without stimuli, which increased to 1450 and 336 Pa (7.8-fold for G', 5.6-fold for G''), respectively, after BAP treatment. The reinforcement may have been caused by increase in the number of cross-linking points and/or pseudo-cross-linking points between fibres in the SDN hydrogel.[41] In sharp contrast, these values decreased almost 100-fold to 2 Pa for G' and 1 Pa for G'' after the addition of $Na_2S_2O_4$. Complete rheological characterisations of the SDN hydrogels are shown in Supplementary Figures 21–25. SDN hydrogels with the different ratios (NPmoc-F(4-F)F: 0.4 wt%, Phos-cycC_6: 0.4 wt%) also showed the same bidirectional control of rheological properties (Supplementary Figure 26). These data clearly demonstrated that the present two-component hydrogel prepared by simple mixing exhibited bidirectional rheological response depending on the applied stimulus. The HPLC analysis of this SDN hydrogel confirmed that

NPmoc-F(4-F)F reacted with $Na_2S_2O_4$, whereas it was unaffected by the BAP treatment (the residual ratio was >95%) (Figure 5d, Supplementary Figure 27). These were in agreement with the results of the CD spectral changes (Supplementary Figure 28). Conversely, **Phos-cycC_6** remained intact after treatment with $Na_2S_2O_4$ and was able to react with BAP (Figure 5d, Supplementary Figure 27). The CD spectral data agreed with the theoretical sum of the BAP-treated single-component **Phos-cycC_6** and **NPmoc-F(4-F)F** (Supplementary Figure 28). Moreover, CLSM images of the resultant hydrogels clearly showed orthogonal fibrous structures (Supplementary Figure 29). This strongly suggested that the original self-sorting fibres retained their orthogonality even after BAP treatment.

On the basis of this unique rheological property, we subsequently applied this SDN hydrogel as a matrix for controlled protein release. After a protein (immunoglobulin G (IgG), myoglobin (Mb), or concanavalin A (ConA)) was encapsulated in the SDN hydrogel, a stimulus ($Na_2S_2O_4$, BAP, or none) was applied to the gel matrix, and proteins release was evaluated using SDS-PAGE of the supernatant solution. As shown in Figure 5e and Supplementary Figure 30, 40±12% of the embedded IgG was slowly released over 10 h without stimulus. Interestingly, IgG release was enhanced by $Na_2S_2O_4$ addition (87±19%), but suppressed by BAP addition (14±2%). Bidirectionally tuned release profiles are also shown for other proteins (Mb and ConA, Figure 5e and Supplementary Figure 31 and 32).

Adaptive response of the SDN hydrogel depending on the order of applied stimuli

We further demonstrated that the bidirectional rheological properties of this SDN hydrogel can produce unprecedented gel–sol transition behaviour depending on the order in which the two stimuli were applied in a stepwise manner (Figure 6a). In these experiments, we applied two stimuli ($Na_2S_2O_4$ and BAP) to the SDN hydrogel in the two different sequences (1^{st} $Na_2S_2O_4$/2^{nd} BAP (route A) or 1^{st} BAP/2^{nd} $Na_2S_2O_4$ (route B)) and observed the macroscopic changes. As shown in Figure 6b, the SDN hydrogel changed to a viscous liquid when $Na_2S_2O_4$ was added first, and the resultant viscous liquid recovered to a hydrogel after subsequent BAP treatment. When the input order was reversed (route B), the hydrogel state remained after each step without appearance of the sol state (Figure 6c). The SDN hydrogel exhibited two distinct response patterns, *i.e.*, the gel–sol–gel for route A and the gel–gel–gel for route B, depending on the order in which the stimuli were applied. This stimulus-order dependent gel-sol change allowed us to encapsulate fluorescent nanobeads under particular conditions. Nanobeads dispersed in aqueous solution were poured on the surface of SDN hydrogels followed by the addition of $Na_2S_2O_4$. After 30 min, the gel was destroyed owing to decomposition of the **NPmoc-F(4-F)F** fibre network, and thus, the beads got immersed in the resultant viscous liquid. The subsequent addition of BAP converted the viscous liquid to a hydrogel again; the nanobeads were encapsulated within the gel matrix (Figure 6f, upper). Conversely, in route B, the gel did not change during any of the stages; therefore, the nanobeads could not be encapsulated (Figure 6f, bottom). Even though the same two stimuli were applied overall, the fluorescent SDN hydrogel encapsulated nanobeads only by the operation of the 1^{st} $Na_2S_2O_4$/2^{nd} BAP stimuli. Therefore, it was concluded that our SDN hydrogel was an adaptive soft-materials capable of recognising the order of input stimuli.[28,29]

This unique macroscopic gel/sol transition was carefully investigated by HPLC analysis, CD spectroscopy and CLSM observation of the Brownian motion of nanobeads. Time-dependent product analyses by HPLC quantitatively showed that the two gelators underwent distinct chemical conversion in each step of the two different routes (Supplementary Figure 33), which corresponded well with the destruction and entanglement of self-sorting supramolecular nanofibres. The CD spectra of SDN hydrogels after the addition of stimuli in different orders were almost identical, which indicated that the final structure was identical irrespective of the stimulus order (Supplementary Figure 34). We also used CLSM to trace the Brownian motion of the 300 nm (diameter) fluorescent beads embedded in the SDN gel matrix (Figure 6d, e, Supplementary movies 2–5). Without stimuli, almost none of the beads moved. In route A, they started to move randomly after the addition of $Na_2S_2O_4$ (Figure 6d, Supplementary movie 2), clearly indicating that the mesh size increased to above 300 nm. Subsequent BAP treatment caused the suppression (almost stoppage) of Brownian motion of the beads, implying that the mesh size reduced to below 300 nm again (Figure 6d, Supplementary movie 3). In route B, all of the fluorescent beads were always stationary, indicating that the mesh size was smaller than 300 nm during all three steps (Figure 6e, Supplementary movies 4, 5). These results revealed that the mesh size was modulated by the sequence in which stimuli were applied.

Conclusions

We have shown a self-sorting supramolecular nanofibre pair, prepared on the basis of the different driving forces for self-assembly of each component. The distinct nanofibres allowed preparation of a rationally designed self-sorting hydrogel with bidirectional rheological and protein release profile changes in response to two orthogonal stimuli. Moreover, the hydrogel exhibited an adaptive gel-sol response by discriminating the order of the stimuli applied. Our hydrogel can be programmed with a desired function, highlighting the utility of self-sorting systems for the bottom-up design of multicomponent intelligent soft materials for a variety of applications including therapy, diagnosis, drug delivery, and regenerative medicine.

References

1. Alberts, B. *et al.* Molecular Biology of the Cell 5th edn, 965–1052 (Garland Science, 2008).
2. Parry, D. A. D. & Squire, J. M. Fibrous proteins: structures and mechanisms (Springer, 2017).
3. Aida, T., Meijer, E. W. & Stupp, S. I. Functional supramolecular polymers. *Science* **335,** 813–817 (2012).
4. Webber, M. J., Appel, E. A., Meijer, E. W. & Langer, R. Supramolecular biomaterials. *Nat. Mater.* **15,** 13–26 (2016).
5. Safont-Sempere, M. M., Fernández, G. & Würthner, F. Self-sorting phenomena in complex supramolecular systems. *Chem. Rev.* **111,** 5784–5814 (2011).
6. Adler-Abramovich, L. & Gazit, E. The physical properties of supramolecular peptide assemblies: from building block association to technological applications. *Chem. Soc. Rev.* **43,** 6881–6893 (2014).
7. Adhikari, B., Nanda, J. & Banerjee, A. Multicomponent hydrogels from enantiomeric amino acid derivatives: helical nanofibers, handedness and self-sorting. *Soft Matter* **7,** 8913–8922 (2011).
8. Buerkle L. E. & Rowan, S. J. Supramolecluar gels formed from multi-component low molecular weight species. *Chem. Soc. Rev.* **41,** 6089–6102 (2012).
9. Shigemitsu, H. & Hamachi, I. Supramolecular assemblies responsive to biomolecules toward biological applications. *Chem. Asian J.* **10,** 2026–2038 (2015).
10. Molla, M. R., Das, A. & Ghosh, S. Self-sorted assembly in a mixture of donor and acceptor chromophores. *Chem. Eur. J.* **16,** 10084–10093 (2010).

11. Smith, M. M. & Smith, D. K. Self-sorting multi-gelator gels–mixing and ageing effects in thermally addressable supramolecular soft nanomaterials. *Soft Matter* **7,** 4856–4860 (2011).

12. Hirst, A. R., Eschder, B., Miravet, J. F. & Smith, D. K. High-tech applications of self-assembling supramolecular nanostructured gel-phase materials: from regenerative medicine to electronic devices. *Angew. Chem. Int. Ed.* **47,** 8002–8018 (2008).

13. Raeburn, J. & Adams, D. J. Multicomponent low molecular weight gelators. *Chem. Commun.* **51,** 5170–5180 (2015).

14. Görl, D., Zhang, X., Stepanenko, V. & Würthner, F. Supramolecular block copolymers by kinetically controlled co-self-assembly of planar and core-twisted perylene bisimides. *Nat. Commun*. **6,** 7009 (2015).

15. Heeres, A. *et al.* Orthogonal self-assembly of low molecular weight hydrogelators and surfactants. *J. Am. Chem. Soc.* **125,** 14252–14253 (2003).

16. Li, C. *et al,* Responsive double network hydrogels of interpenetrating DNA and CB[8] Host-Guest supramolecular systems. *Adv. Mater.* **27,** 3298–3304 (2015).

17. Colquhoun, C. *et al.* The effect of self-sorting and co-assembly on the mechanical properties of low molecular weight hydrogels. *Nanoscale* **6,** 13719–13725 (2014).

18. Pal, A., Besenius, P. & Sijbesma, R. P. Self-sorting in rodlike micelles of chiral bisurea bolaamphiphiles. *J. Am. Chem. Soc.* **133,** 12987–12989 (2011).

19. Draper, E. R., Jonathan, R. L., Wallace, M., Jäckel, F., Cowan, A. J., Adams, D. J. Self-sorted photoconductive xerogels. *Chem. Sci.* **7,** 6499–6505 (2016).

20. Boekhoven, J., Koot, M., Wezendonk, T. A., Eelkema, R. & van Esch, J. H. A self assembled delivery platform with post-production tunable release rate. *J. Am. Chem. Soc.* **134,** 12908–12911 (2012).

21. Morris, K. L. *et al.* Chemically programmed self-sorting of gelator networks. *Nat. Commun*. **4,** 1480 (2013).

22. Draper, E. R., Eden, E. G. B., McDonald, T. O. & Adams, D. J. Spatially resolved multicomponent gels. *Nat. Chem.* **7,** 848–852 (2015).

23. Cornwell D. J., Daubney O. J. & Smith D. K. Photopatterned multidomain gels: multi-component self-assembled hydrogels based on partially self-sorting 1,3:2,4-Dibenzylidene-*d*-sorbitol derivatives. *J. Am. Chem. Soc.* **137**, 15486–15492 (2015).

24. Singh, N. *et al.* Tandem reactions in self-sorted catalytic molecular hydrogels. *Chem. Sci.* **7,** 5568–5572 (2016).

25. Sugiyasu, K., Kawano, S.-i., Fujita, N. & Shinkai, S. Self-sorting organogels with p–n heterojunction points. *Chem. Mater.* **20,** 2863–2865 (2008).

26. Prasanthkumar, S. *et al.* Organic donor–acceptor assemblies form coaxial p–n heterojunctions with high photoconductivity. *Angew. Chem. Int. Ed.* **54,** 946–950 (2015).

27. Cornwell, D. J. & Smith, D. K. Expanding the scope of gels – combining polymers with low-molecular weight gelators to yield modified self-assembling smart materials with high-tech applications. *Mater. Horiz*. **2,** 279–293 (2015).

28. Ikeda, M. *et al.* Installing logic-gate responses to a variety of biological substances in supramolecular hydrogel–enzyme hybrids. *Nat. Chem.* **6,** 511–518 (2014).

29. Komatsu, H. *et al.* Supramolecular hydrogel exhibiting four basic logic gate functions to fine-tune substance release. *J. Am. Chem. Soc.* **131,** 5580–5585 (2009).

30. S. Onogi *et al. In situ* real-time imaging of self-sorted supramolecular nanofibres. *Nat. Chem.* **8,** 743–752 (2016).

31. Boekhoven, J. *et al.* Bio-inspired supramolecular materials by orthogonal self-assembly of hydrogelators and phospholipids. *Chem. Sci.* **7,** 6021–6031 (2016).

32. Ikeda, M., Tanida, T., Yoshii, T. & Hamachi, I. Rational molecular design of stimulus-responsive supramolecular hydrogel based on dipeptides. *Adv. Mater.* **23,** 2819–2822 (2011).

33. Shigemitsu, H. *et al.* Preparation of supramolecular hydrogel–enzyme hybrids exhibiting biomolecule-responsive gel degradation. *Nat. Protoc*. **11,** 1744–1756 (2016).

34. Kiyonaka, S., Sugiyasu, K., Shinkai, S. & Hamachi, I. First thermally responsive supramolecular polymer based on glycosylated amino acid. *J. Am. Chem. Soc.* **124,** 10954–10955 (2002).

35. Dunn, K.W., Kamocka, M. M. & McDonald, J. H. A practical guide to evaluating colocalization in biological microscopy. *Am. J. Physiol. Cell Physiol.* **300,** C723–C742 (2011).

36. Tamaru, S.-i. *et al.* Fluidic supramolecular nano- and microfibres as molecular rails for regulated movement of nanosubstances. *Nat. Commun.* **1,** 20 (2010).

37. Thompson, N. L., Burghardt, T. P. & Axelrod, D. Measuring surface dynamics of biomolecules by total internal reflection fluorescence with photobleaching recovery or correlation spectroscopy. *Biophys. J.* **33,** 435–454 (1981).

38. Jayaraman, K. *et al.* Observing capillarity in hydrophobic silica nanotubes. *J. Am. Chem. Soc.* **127,** 17385–17392 (2005).

39. Matsumoto, S. *et al.* Photo gel–sol/sol–gel transition and its patterning of a supramolecular hydrogel as stimuli-responsive biomaterials. *Chem. Eur. J.* **14,** 3977–3986 (2008).

40. Yoshii, T., Ikeda, M. & Hamachi, I., Two-photon-responsive supramolecular hydrogel for controlling materials motion in micrometer space. *Angew. Chem. Int. Ed.* **53,** 7264–7267 (2014).

41. Shams Es-haghi, S. & Weiss, R. A. Fabrication of tough hydrogels from chemically cross-linked multiple neutral networks. *Macromolecules*, **49,** 8980–8987 (2016).

Acknowledgements

The authors thank M. Suginome and Y. Nagata (Kyoto University) for CD spectra measurements, N. Yamada (Kyoto Insititute of Technology) for their kind support with rheological measurements, and Y. Sato (Carl Zeiss Microimaging Co.) for CLSM imaging with Airyscan unit. H. S. acknowledges JSPS Research Fellowships for Young Scientists (16J10716). The authors acknowledge financial support from The Mitsubishi foundation.

Author contributions

H. S. and I. H. conceived the project and designed the experiments. H. S., T. F., and W. T. performed all the experiments. H. S., S. M. and K. U. analyzed rheological properties. The paper was written by H. S., R. K., and I. H. and edited by all the co-authors.

Competing financial interests

The authors declare no competing financial interests.

1 **Figure Captions**

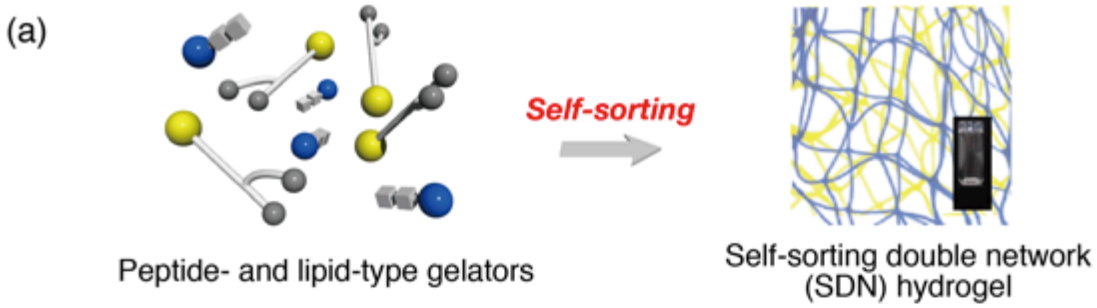

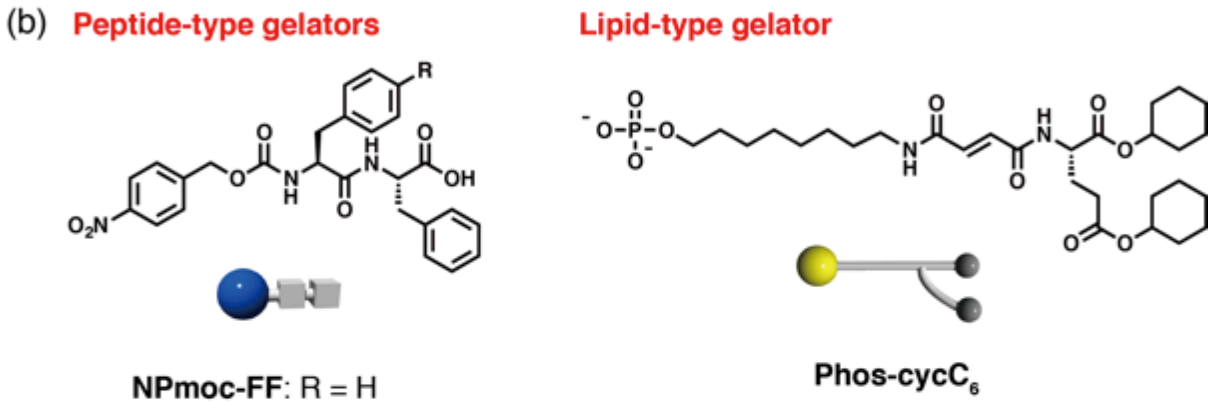

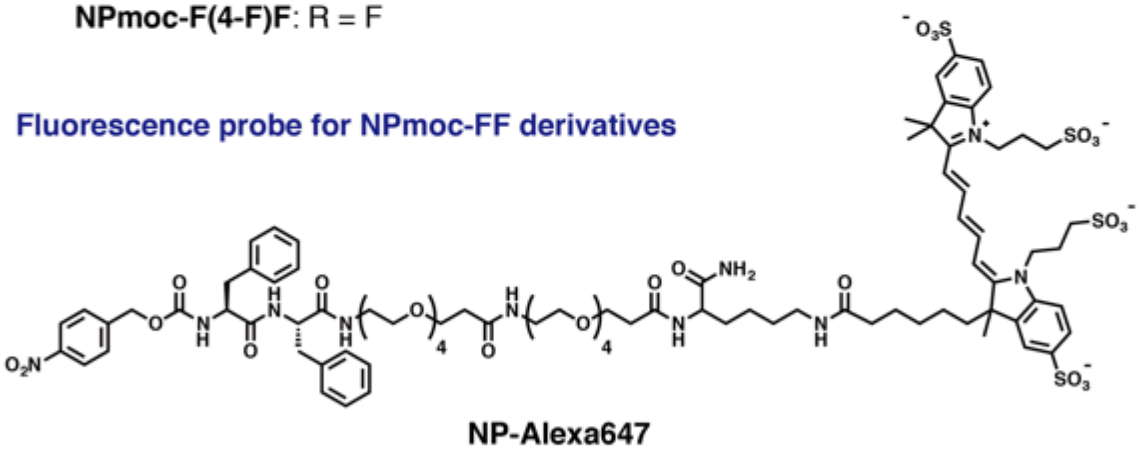

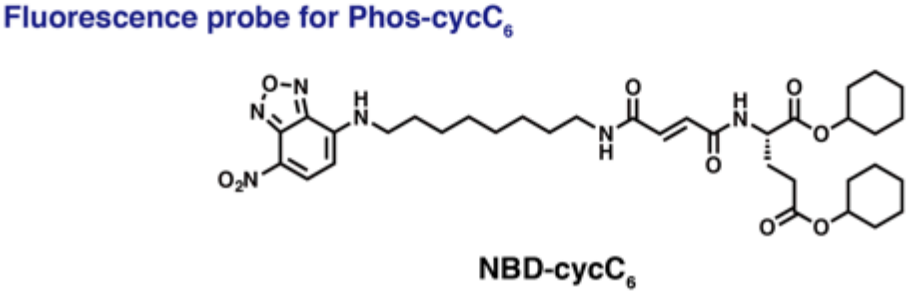

2

Figure 1. **Schematic representation of formation of a self-sorting double network (SDN) hydrogel, and molecular structures of hydrogelators and fluorescence probes.** (a) Two low molecular weight peptide- and lipid-type hydrogelators orthogonally assemble into two distinct supramolecular nanofibres and form a SDN hydrogel. The SDN hydrogel shows the adaptive functions such as bidirectional control of rheological property and release rate of encapsulated molecules by specific external stimuli. The peptide- and lipid-type hydrogelators are described as schematic blue and yellow molecules, respectively. The blue and yellow networks shown in the right indicate nanofibres consisting of self-assembled peptide- and lipid-type hydrogelators, respectively. (b) Chemical structures of peptide- and lipid-type gelators (**NPmoc-FF**, **NPmoc-F(4-F)F**, and **Phos-cycC_6**) and fluorescence probes (**NP-Alexa647** and **NBD-cycC_6**) which selectively stain self-sorting supramolecular nanofibres and enable *in situ* CLSM imaging.

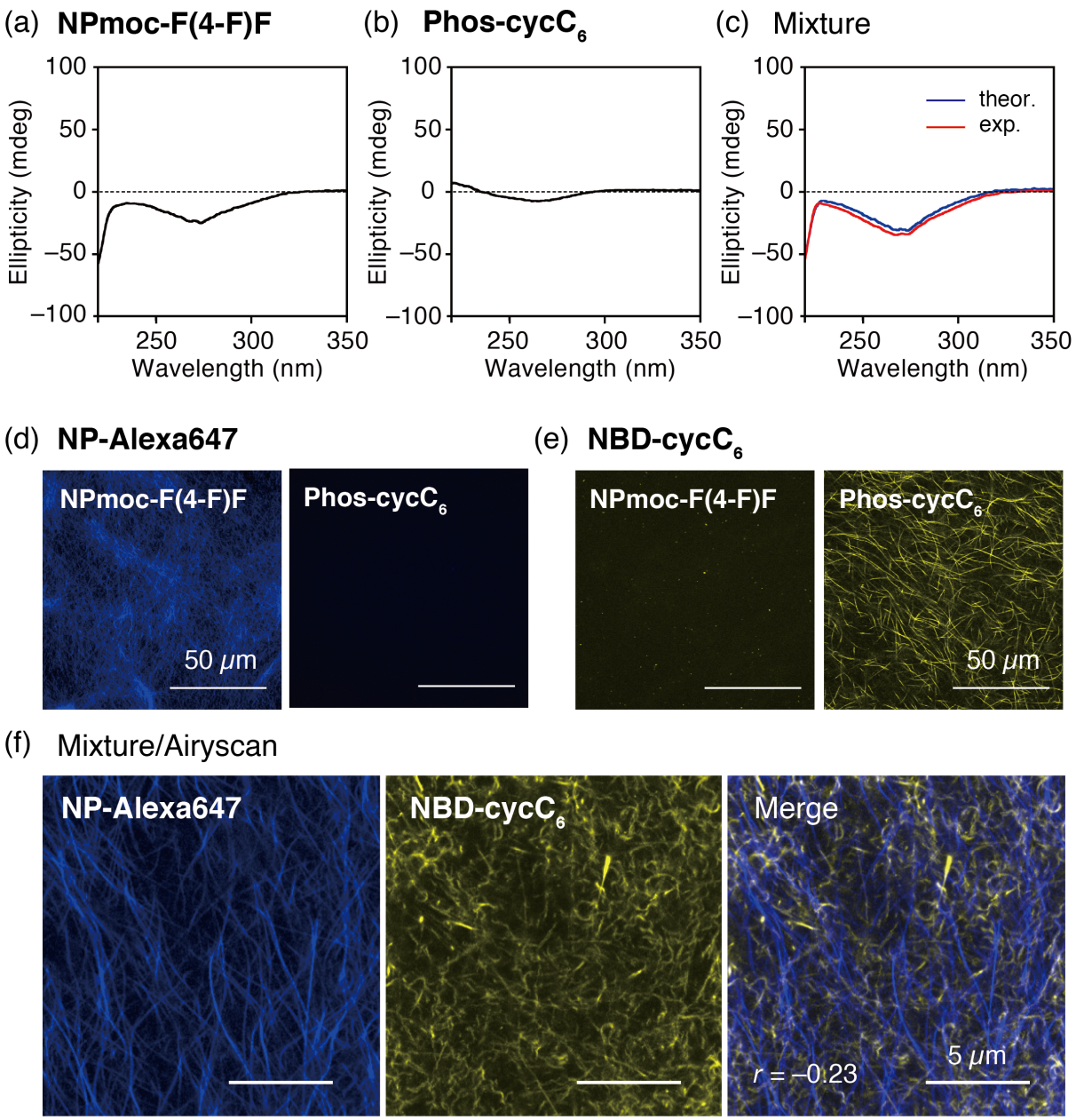
(a) NPmoc-F(4-F)F
(b) Phos-cycC6
(c) Mixture
Ellipticity (mdeg)
100
50
0
−50
−100
250
300
350
Wavelength (nm)
theor.
exp.
(d) NP-Alexa647
NPmoc-F(4-F)F
Phos-cycC6
50 μm
(e) NBD-cycC6
NPmoc-F(4-F)F
Phos-cycC6
50 μm
(f) Mixture/Airyscan
NP-Alexa647
NBD-cycC6
Merge
r = −0.23
5 μm

1

Figure 2. **Evaluation for self-sorting of NPmoc-F(4-F)F and Phos-cycC_6.** (a–c) CD spectra of **NPmoc-F(4-F)F** (a), **Phos-cycC_6** (b), and a mixture of **NPmoc-F(4-F)F** and **Phos-cycC_6** (c). The blue and red lines in (c) show theoretical and experimental CD spectra, respectively. The theoretical CD spectrum is a simple sum of the CD spectra of **NPmoc-F(4-F)F** and **Phos-cycC_6** ((a) and (b)). The HT data is shown in Supplementary Figures 5 and 6. CD spectra measured under different conditions also shown in Supplementary Figure 7. (d, e) CLSM images of **NPmoc-F(4-F)F** and **Phos-cycC_6** supramolecular nanofibres in the presence of **NP-Alexa647** (d) and **NBD-cycC_6** (e). (f) High-resolution CLSM (with Airyscan unit) images of self-sorting **NPmoc-F(4-F)F** and **Phos-cycC_6** fibres stained by **NP-Alexa647** and **NBD-cycC_6**, respectively. The left, middle, and right images show **NPmoc-F(4-F)F**, **Phos-cycC_6** fibres and the merged images, respectively. The number in the merged image is the Pearson correlation coefficient value (*r*). Scale bar: 5 μm. Conditions: [**NPmoc-F(4-F)F**] = 0.40 wt% (7.9 mM), [**Phos-cycC_6**] = 0.15 wt% (2.4 mM), [**NP-Alexa647**] = 4.0 μM, [**NBD-cycC_6**] = 20 μM in 100 mM HEPES buffer (pH 8.0), rt.

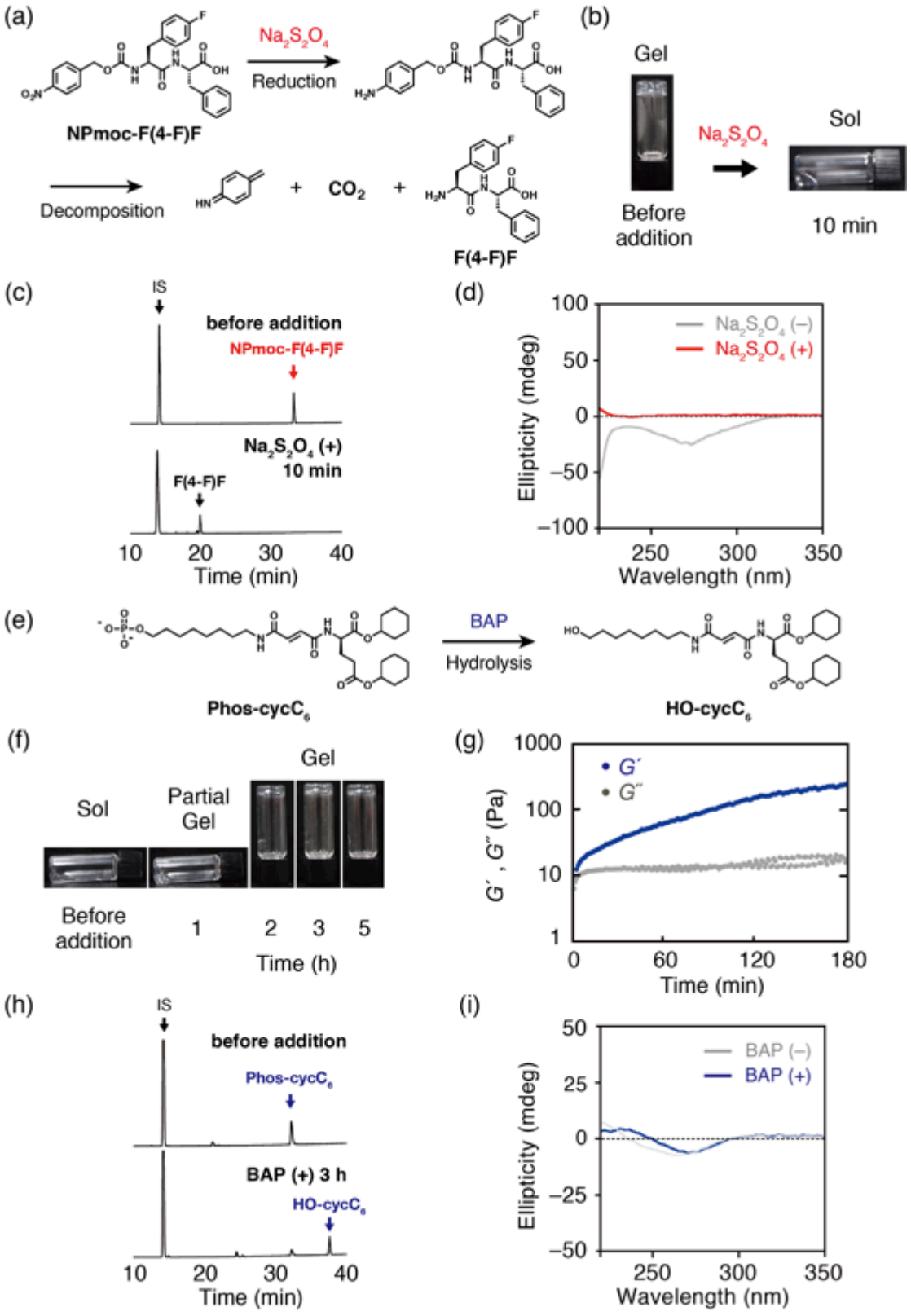
(a)
$Na_2S_2O_4$
Reduction
NPmoc-F(4-F)F
Decomposition
+ CO_2 +
F(4-F)F
(b)
Gel
$Na_2S_2O_4$
Sol
Before addition
10 min
(c)
IS
before addition
NPmoc-F(4-F)F
$Na_2S_2O_4$ (+)
10 min
F(4-F)F
Time (min)
(d)
$Na_2S_2O_4$ (–)
$Na_2S_2O_4$ (+)
Ellipticity (mdeg)
Wavelength (nm)
(e)
BAP
Hydrolysis
Phos-cycC$_6$
HO-cycC$_6$
(f)
Gel
Sol
Partial Gel
Before addition
Time (h)
(g)
G′
G″
G′ , G″ (Pa)
Time (min)
(h)
IS
before addition
Phos-cycC$_6$
BAP (+) 3 h
HO-cycC$_6$
Time (min)
(i)
BAP (–)
BAP (+)
Ellipticity (mdeg)
Wavelength (nm)

1

Figure 3. **Stimuli responsiveness of NPmoc-F(4-F)F and Phos-cycC_6 ((a)–(d): NPmoc-F(4-F)F, (e)–(i): Phos-cycC_6).** (a) Chemical reaction between **NPmoc-F(4-F)F** and $Na_2S_2O_4$. The nitro group is reduced by $Na_2S_2O_4$ and the generated aniline derivative spontaneously decomposes. (b) Optical photos of **NPmoc-F(4-F)F** gel and the sol after addition of $Na_2S_2O_4$ (10 min). (c) HPLC charts of **NPmoc-F(4-F)F** gel before and after addition of $Na_2S_2O_4$ (10 min). (d) CD spectra of **NPmoc-F(4-F)F** gel (gray) and the sol obtained from **NPmoc-F(4-F)F** gel by addition of $Na_2S_2O_4$ (red). Conditions: [**NPmoc-F(4-F)F**] = 0.40 wt% (7.9 mM), [$Na_2S_2O_4$] = 79 mM (10 eq. for **NPmoc-F(4-F)F**) in 100 mM HEPES buffer (pH 8.0). $V_{gel}/V_{Na_2S_2O_4\ aq.}$ = 10:1, 25 ºC, 10 min. (e) Chemical reaction between **Phos-cycC_6** and BAP. (f) Optical photos of **Phos-cycC_6** solution after addition of BAP. (g) Time-course of the rheological properties of the **Phos-cycC_6** solution after addition of BAP (0–180 min). (h) HPLC charts of **Phos-cycC_6** solution or gel after addition of BAP (3 h). (i) CD spectra of **Phos-cycC_6** solution and the gel obtained by addition of BAP. Conditions: [**Phos-cycC_6**] = 0.15 wt% (2.4 mM), [BAP] = 0.05 U/μL in 100 mM HEPES buffer (pH 8.0). V_{gel}/V_{BAP} = 10:1, 25 ºC, 300 min. IS in figures (c) and (h) mean internal standard (terephthalic acid).

(a)

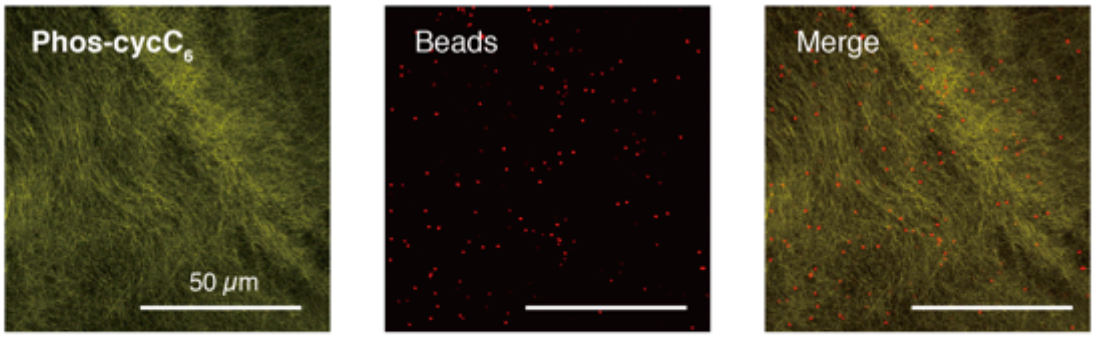

(b) BAP (–)

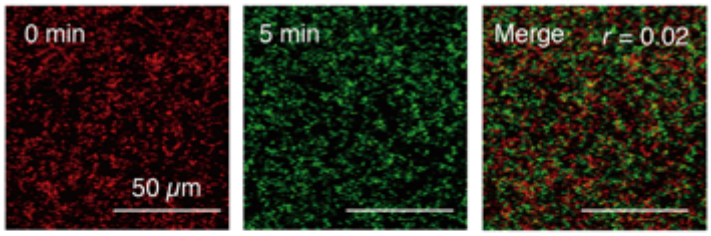

BAP (+), 3 h

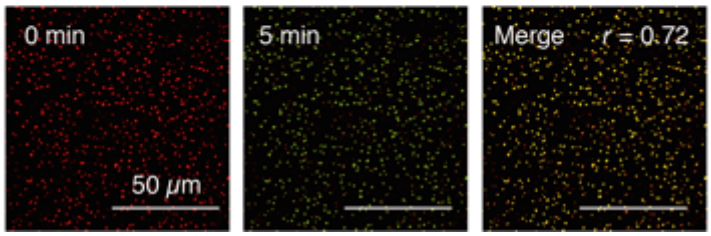

(c)

Beads diameter (nm)	BAP –	BAP +
70	ON	ON
200	ON	ON / OFF
300	ON	OFF
500	ON	OFF
800	OFF	OFF

1

Figure 4. **Brownian motions of beads in Phos-cycC_6 sol or gel generated by BAP treatment.** (a) CLSM images of the mixture of **Phos-cycC_6** and fluorescent beads (800 nm) in buffer solution. The right, middle, and left images show **Phos-cycC_6** fibres stained with **NBD-cycC_6**, fluorescent beads and the merged image, respectively. Scale bar: 50 μm. (b) CLSM images of the Brownian motions of beads (diameter: 300 nm) in **Phos-cycC_6** sol and gel. The red (left) and green (middle) CLSM images show the positions of the fluorescence beads at 0 and 5 min after starting the observation. The right images show the combined images. In the images, the yellow beads indicate that the positions of the beads did not change at 0 and 5 min after starting the observations. The numbers in the images represent Pearson correlation coefficient (*r*). The movie of the Brownian motions of the beads can be seen in supplementary movie S1. Scale bar: 25 μm. (c) Brownian motions of beads (diameter: 70–800 nm) in **Phos-cycC_6** solution and the gel after addition of BAP (3 h). Conditions: [**Phos-cycC_6**] = 0.15 wt% (2.4 mM), [**NBD-cycC_6**] = 20 μM, [BAP] = 0.05 U/μL. [Fluorescence nanobeads (300 nm)] = 0.05 mg/mL in 100 mM HEPES buffer (pH 8.0). V_{gel}/V_{BAP} = 10:1, 25 ºC, 3 h.

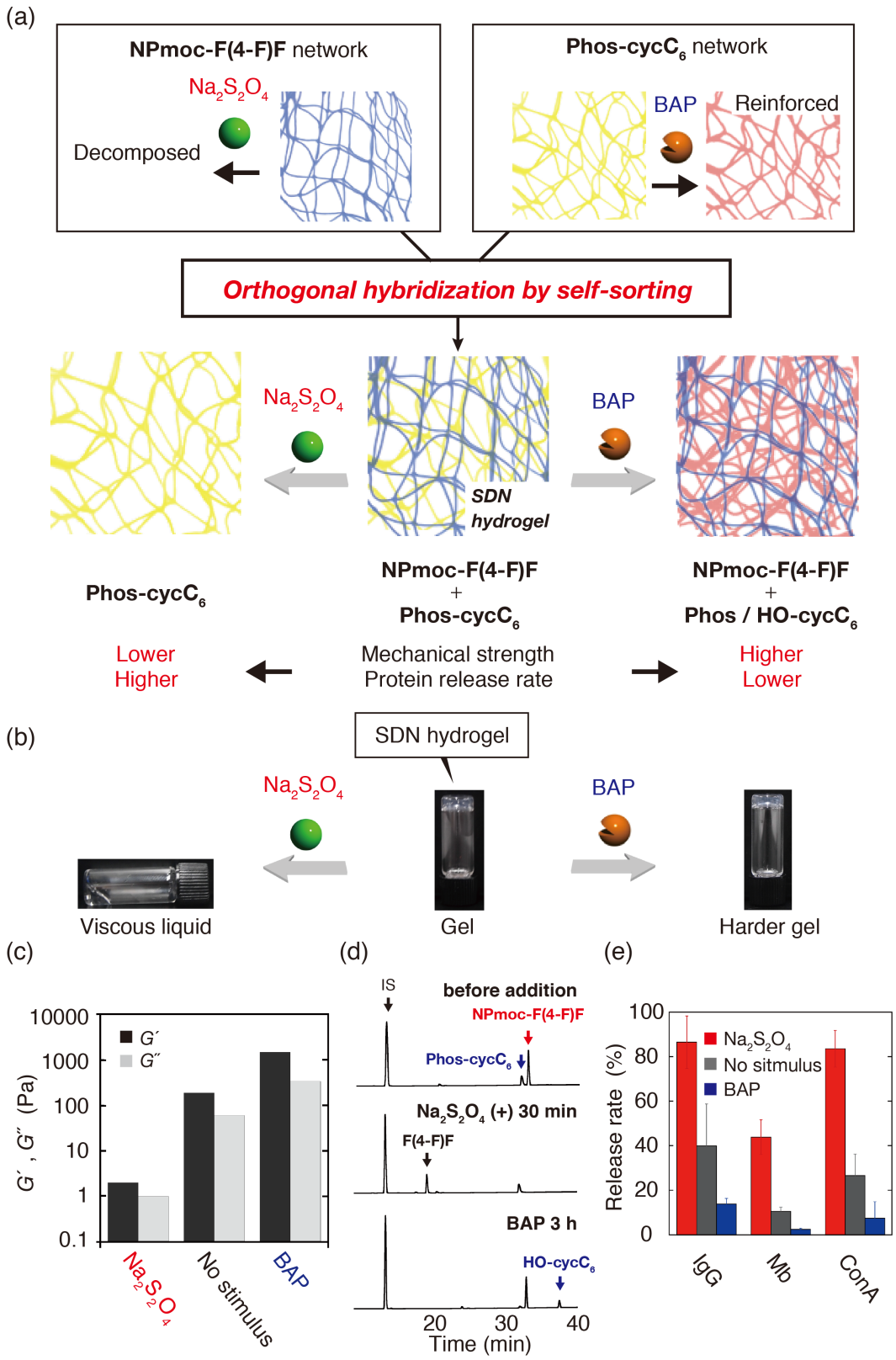
(a)
NPmoc-F(4-F)F network
Na2S2O4
Decomposed
Phos-cycC6 network
BAP
Reinforced
Orthogonal hybridization by self-sorting
Na2S2O4
BAP
SDN hydrogel
Phos-cycC6
NPmoc-F(4-F)F + Phos-cycC6
NPmoc-F(4-F)F + Phos / HO-cycC6
Lower Higher
Mechanical strength Protein release rate
Higher Lower
(b)
SDN hydrogel
Na2S2O4
BAP
Viscous liquid
Gel
Harder gel
(c)
(d)
(e)
10000
1000
100
10
1
0.1
G´ , G˝ (Pa)
G´
G˝
Na2S2O4
No stimulus
BAP
IS
before addition
NPmoc-F(4-F)F
Phos-cycC6
Na2S2O4 (+) 30 min
F(4-F)F
BAP 3 h
HO-cycC6
20
30
40
Time (min)
100
80
60
40
20
0
Release rate (%)
Na2S2O4
No sitmulus
BAP
IgG
Mb
ConA

1

Figure 5. **Stimuli-responsiveness of the self-sorting double network (SDN) hydrogel.** (a) Schematic representation of orthogonal hybridization of the expected responses towards $Na_2S_2O_4$ and BAP into the SDN hydrogel. The blue, yellow, and red colours indicate **NPmoc-F(4-F)F**, **Phos-cycC_6**, and **Phos** / **HO-cycC_6** networks, respectively. (b) Optical photos of the SDN hydrogels (middle) and the viscous liquid and gel after addition of $Na_2S_2O_4$ (left) and BAP (right), respectively. (c) Rheological properties of the SDN hydrogel at a frequency of 10 rad/s before and after addition of stimuli (left: $Na_2S_2O_4$ (30 min), middle: no stimulus, right: BAP (3 h)). The control experiments, the frequency dependences of the gel samples and the reason of larger G' than G'' of the viscous liquid obtained after addition of $Na_2S_2O_4$ to the SDN hydrogel are shown and discussed in Supplementary Figures 21–25. (d) HPLC charts of the SDN hydrogels (upper: before addition, middle: $Na_2S_2O_4$ (30 min), lower: BAP (3 h)). (e) Protein release rate from the SDN hydrogels after addition of stimuli (left: IgG, middle: Mb, right: ConA, red: $Na_2S_2O_4$ (30 min), gray: no stimulus, blue: BAP (3 h)). The data represent mean ± s.d.m (n = 3). Conditions: [**NPmocF(4-F)F**] = 0.40 wt% (7.9 mM), [**Phos-cycC_6**] = 0.15 wt% (2.4 mM), [$Na_2S_2O_4$] = 79 mM (10 eq. for **NPmoc-F(4-F)F**), [BAP] = 0.05 U/μL for (b,c,d) and 0.005 U/μL for (e) in 100 mM HEPES buffer (pH 8.0). $V_{gel}/V_{stimulus}$ = 10:1, 25 ºC. In Figure (e), the protein stock solutions (0.5 mg/mL IgG, 1.0 mg/mL ConA, 0.5 mg/mL myoglobin, 10 μL) were added to SDN hydrogels (200 μL).

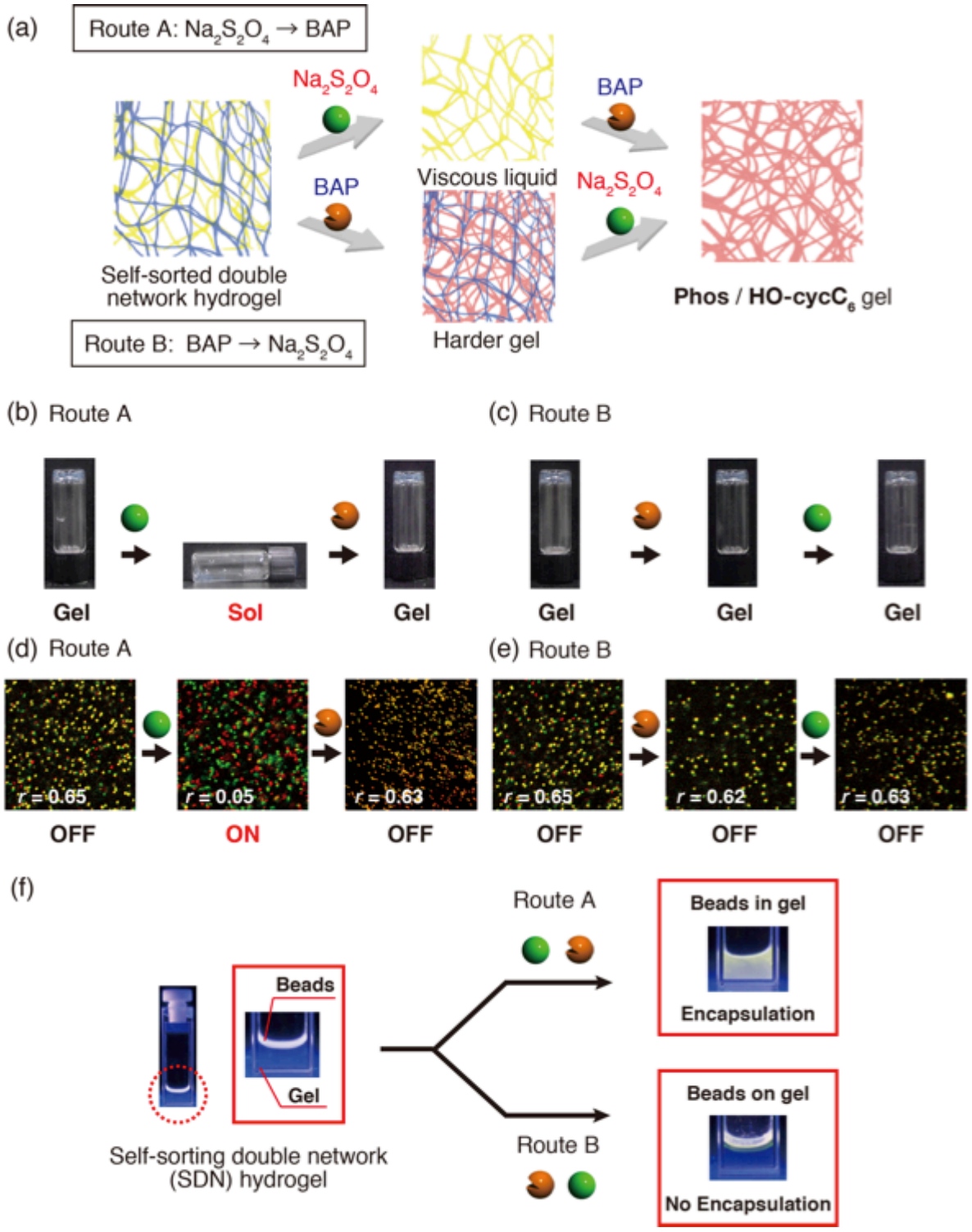
(a)
Route A: $Na_2S_2O_4$ → BAP
$Na_2S_2O_4$
BAP
Viscous liquid
BAP
$Na_2S_2O_4$
Self-sorted double network hydrogel
Harder gel
Phos / HO-cycC$_6$ gel
Route B: BAP → $Na_2S_2O_4$
(b) Route A
(c) Route B
Gel
Sol
Gel
Gel
Gel
Gel
(d) Route A
(e) Route B
r = 0.65
r = 0.05
r = 0.63
r = 0.65
r = 0.62
r = 0.63
OFF
ON
OFF
OFF
OFF
OFF
(f)
Route A
Beads in gel
Beads
Gel
Encapsulation
Self-sorting double network (SDN) hydrogel
Route B
Beads on gel
No Encapsulation

1

Figure 6. **Recognition of the stimulus order by the SDN hydrogel.** (a) Schematic representation of recognition of the stimulus order by the SDN hydrogels. The upper line shows the expected changes of the SDN hydrogel after addition of $Na_2S_2O_4$ and then BAP (route A). The lower line shows the reverse addition order (route B). The blue, yellow, and red colours indicate **NPmoc-F(4-F)F**, **Phos-cycC$_6$**, and **Phos** / **HO-cycC$_6$** networks, respectively. (b, c) Optical photos of the SDN hydrogels after addition of stimuli (b: route A, c: route B). (d, e) Brownian motion of beads (diameter: 300 nm) in the SDN hydrogels before and after addition of stimuli (d: route A, e: route B). The images are merged images at 0 and 1 min after starting CLSM observations. The original CLSM images at 0 and 1 min are shown in Supplementary Figures 35 and 36. The numbers in the images represent Pearson's correlation coefficient (*r*). [Fluorescence nanobeads (300 nm)] = 0.05 mg/mL. (f) Optical photos of bead encapsulation experiments (upper: route A, lower: route B) under UV light (254 nm). The left photo in a red box shows the magnified image of the hydrogel and fluorescence beads before addition of stimuli. The right photos indicate the hydrogels after addition of stimuli (upper: route A, lower: route B). In the case of route A, fluorescence beads were encapsulated in the resultant hydrogels. On the other hand, in route B, the beads were not encapsulated in the hydrogels. Conditions: [**NPmocF(4-F)F**] = 0.40 wt% (7.9 mM), [**Phos-cycC$_6$**] = 0.15 wt% (2.4 mM), [$Na_2S_2O_4$] = 79 mM (10 eq. for **NPmoc-F(4-F)F**), [BAP] = 0.05 U/μL in 100 mM HEPES buffer (pH 8.0). $V_{gel}/V_{stimulus}$ = 10:1, 25 ºC.

Methods

The materials, instruments, experimental methods and syntheses of the compounds are described in supplementary material. The conditions (concentration, pH and temperature) of the experiments are provided in the figure captions. The authors declare that the data that support the findings of this study are available within this paper and its supplementary information files.

Additional information

Supplementary information is available in the online version of the paper. Reprints and permission information is available online at www.nature.com/reprints. Correspondence and requests for materials should be addressed to I. H.